

CONSTRAINING THE EARLY-UNIVERSE BARYON DENSITY AND EXPANSION RATE

VIMAL SIMHA¹ AND GARY STEIGMAN²
Draft version October 23, 2018

ABSTRACT

We explore the constraints on those extensions to the standard models of cosmology and particle physics which modify the early-Universe, radiation-dominated, expansion rate $S \equiv H'/H$ (parametrized by the effective number of neutrinos N_ν). The constraints on S (N_ν) and the baryon density parameter $\eta_B \equiv (n_B/n_\gamma) = 10^{-10}\eta_{10}$, derived from Big Bang Nucleosynthesis (BBN, $t \sim 20$ minutes) are compared with those inferred from the Cosmic Microwave Background Anisotropy spectrum (CMB, $t \sim 400$ kyr) and Large Scale Structure (LSS, $t \sim 14$ Gyr). At present, BBN provides the strongest constraint on N_ν ($N_\nu = 2.4 \pm 0.4$ at 68% confidence), but a weaker constraint on the baryon density. In contrast, while the CMB/LSS data best constrain the baryon density ($\eta_{10} = 6.1^{+0.2}_{-0.1}$ at 68% confidence), independent of N_ν , at present they provide a relatively weak constraint on N_ν which is, however, consistent with the standard value of $N_\nu = 3$. When the best fit values and the allowed ranges of these CMB/LSS-derived parameters are used to calculate the BBN-predicted primordial abundances, there is excellent agreement with the observationally inferred abundance of deuterium and good agreement with ^4He , confirming the consistency between the BBN and CMB/LSS results. However, the BBN-predicted abundance of ^7Li is high, by a factor of 3 or more, if its observed value is uncorrected for possible dilution, depletion, or gravitational settling. We comment on the relation between the value of N_ν and a possible anomaly in the matter power spectrum inferred from observations of the Ly- α forest. Comparing our BBN and CMB/LSS results permits us to constrain any post-BBN entropy production as well as the production of any non-thermalized relativistic particles. The good agreement between our BBN and CMB/LSS results for N_ν and η_B permits us to combine our constraints finding, at 95% confidence, $1.8 < N_\nu < 3.2$ and $5.9 < \eta_{10} < 6.4$.

Subject headings: neutrinos — early universe — expansion rate — baryon density

1. INTRODUCTION

The standard models of particle physics and of cosmology with dark energy, baryonic matter, radiation (including three species of light neutrinos), and dark matter is consistent with cosmological data from several widely-separated epochs. However, there is room to accommodate some models of non-standard physics within the context of this well tested, Λ CDM cosmology. One possibility, explored here, is that of a non-standard expansion rate ($S \equiv H'/H$, where H is the Hubble parameter) during the early, radiation-dominated evolution of the Universe driven perhaps, but not necessarily, by a non-standard content of relativistic particles ($\rho'_R \neq \rho_R$), parametrized by the equivalent number of additional neutrinos ($\rho'_R \equiv \rho_R + \Delta N_\nu \rho_\nu$, where $\Delta N_\nu \equiv N_\nu - 3$ prior to the epoch of e^\pm annihilation). In the epoch just prior to e^\pm annihilation, which is best probed by Big Bang Nucleosynthesis (BBN), $\rho_R = \rho_\gamma + \rho_e + 3\rho_\nu = 43\rho_\gamma/8$, so that

$$S^2 \equiv \left(\frac{H'}{H}\right)^2 \equiv \frac{\rho'_R}{\rho_R} \equiv 1 + \frac{7\Delta N_\nu}{43}. \quad (1)$$

In the epoch after the completion of e^\pm annihilation, best probed by the Cosmic Microwave Background (CMB) and by Large Scale Structure (LSS), the relations between ρ_R and ρ_γ and between S and ΔN_ν differ from those in eq. 1, as described below in some detail in §2.

We use the comparison between the predicted and observed abundances of the light elements produced during BBN, and between the predicted and observed CMB anisotropy spectrum, along with data from LSS observed in the present/recent Universe, to constrain new physics which leads to a non-standard, early-Universe expansion rate (S) or, equivalently, to place bounds on the effective number of neutrinos (N_ν); for related earlier work see, e.g., Barger et al. (2003); Cyburt (2004). In addition, the baryon density and, any variation in it over widely-separated epochs in the evolution of the Universe, are constrained simultaneously with N_ν , thereby testing the standard-model expectation that the ratio (by number) of baryons to CMB photons ($\eta_B \equiv n_B/n_\gamma$) should be unchanged from e^\pm annihilation ($T \lesssim 1/2$ MeV; $t \gtrsim 3$ s) until the present ($T = 2.725$ K $\approx 2 \times 10^{-10}$ MeV, $t \approx 14$ Gyr).

In §2 a non-standard expansion rate (S) is related to a non-standard radiation density, parametrized by an effective number of neutrinos N_ν . In §3, the observationally inferred primordial light element (D, ^4He , ^7Li) abundances are used to constrain the radiation density (expansion rate) and the baryon density. In §4, we assume a flat, Λ CDM cosmology and use data from the CMB, along with a prior on the Hubble parameter from the HST key project, luminosity distances of type Ia supernovae, and the matter power spectrum to provide independent constraints on the radiation density and the baryon density. The results from these two epochs, very widely-separated in time, are compared constraining any post-BBN entropy production. The good agreement

¹ Department of Astronomy, The Ohio State University, 140 West 18th Ave., Columbus, OH 43210

² Departments of Physics and Astronomy and Center for Cosmology and Astro-Particle Physics, The Ohio State University, 191 West Woodruff Ave., Columbus, OH 43210

between them permits us to combine them to obtain a joint constraint on the baryon density parameter (η_B) and the effective number of neutrinos (N_ν).

2. NON-STANDARD EARLY-UNIVERSE EXPANSION RATE OR RADIATION DENSITY

In the radiation-dominated early universe ($\rho_{\text{TOT}} \rightarrow \rho_R$) the expansion rate (H) is related to the radiation density through the Friedman equation.

$$H^2 = \frac{8\pi}{3} G \rho_R. \quad (2)$$

Any modification to the radiation density, or to the Friedman equation by a term which evolves like the radiation density (as the inverse fourth power of the scale factor) can be parametrized by an equivalent number of additional neutrinos ΔN_ν where, prior to e^\pm annihilation, $\Delta N_\nu \equiv N_\nu - 3$. For the standard models of particle physics and cosmology, in the epoch after muon annihilation ($T \lesssim 100$ MeV) and prior to e^\pm annihilation ($T \gtrsim 0.5$ MeV), the radiation consists of an equilibrium mixture of photons, relativistic e^\pm pairs, and three flavors of extremely relativistic, left-handed neutrinos (and their right-handed, antineutrino counterparts). In this case, the total radiation density may be written in terms of the photon density as

$$\rho_R = \frac{43}{8} \rho_\gamma = 5.375 \rho_\gamma. \quad (3)$$

In this same epoch, prior to e^\pm annihilation, a modified radiation density can be written as

$$\rho'_R = \rho_R \left(1 + \frac{7\Delta N_\nu}{43} \right) = \rho_R (1 + 0.163 \Delta N_\nu) \quad (4)$$

where ρ_R is the standard-model radiation energy density and ρ'_R is the modified, non-standard model radiation energy density. In a sense, this modified energy density is simply a proxy for a non-standard expansion rate during the radiation-dominated epoch relevant for comparison with BBN.

$$S \equiv \frac{H'}{H} = \left(\frac{\rho'_R}{\rho_R} \right)^{1/2} = \left(1 + \frac{7\Delta N_\nu}{43} \right)^{1/2}. \quad (5)$$

After e^\pm annihilation the surviving relativistic particles are the photons (which will redshift to the presently observed CMB) and the now decoupled, relic neutrinos. In the approximation that the neutrinos are fully decoupled at e^\pm annihilation, the post- e^\pm annihilation photons are hotter than the neutrinos by a factor of $T_\gamma/T_\nu = (11/4)^{1/3}$ and

$$\rho_R = \left[1 + 3 \times \frac{7}{8} \left(\frac{4}{11} \right)^{4/3} \right] \rho_\gamma = (1 + 3 \times 0.227) \rho_\gamma = 1.681 \rho_\gamma, \quad (6)$$

so that

$$\rho'_R = \rho_\gamma (1.681 + 0.227 \Delta N_\nu) = \rho_R (1 + 0.135 \Delta N_\nu), \quad (7)$$

where, as before, $\Delta N_\nu \equiv N_\nu - 3$.

However, it is well known (Dicus et al. 1982; Dodelson & Turner 1992; Hannestad & Madsen 1995; Lopez et al. 1999; Dolgov 2002) that the standard-model neutrinos are not fully decoupled at e^\pm annihilation. As a result, the relic neutrinos share some of the energy/entropy released by e^\pm annihilation and they are warmer than in the fully decoupled approximation, increasing the ratio of the post- e^\pm annihilation radiation density to the photon energy density. While the post- e^\pm annihilation phase space distribution of the decoupled neutrinos is no longer that of a relativistic, Fermi-Dirac gas, according to Mangano et al. (2005) the additional contribution to the total energy density can be accounted for by replacing $N_\nu = 3$ with $N_\nu = 3.046$, so that

$$\rho_R \rightarrow (1 + 3.046 \times 0.227) \rho_\gamma = 1.692 \rho_\gamma. \quad (8)$$

For deviations from the standard model that can be treated as equivalent to contributions from fully decoupled neutrinos,

$$\rho'_R = \rho_R (1 + 0.134 \Delta N_\nu), \quad (9)$$

where $\Delta N_\nu \equiv N'_\nu - 3.046$ in the post- e^\pm annihilation Universe relevant for comparison with the CMB and LSS. Note that in the standard model, where $N_\nu = 3$ prior to e^\pm annihilation, the neutrino contribution to the post- e^\pm annihilation radiation energy density is equivalent to $N'_\nu = 3.046$, so that for the standard models of cosmology (standard expansion rate) and of particle physics (standard radiation energy density), $N_\nu = 3$, $N'_\nu = 3.046$ and, $\Delta N_\nu = 0$.

We emphasize that although the non-standard radiation density (expansion rate) has been parametrized as if it were due to additional species of neutrinos, this parametrization accounts for any term in the Friedman equation whose energy density varies as a^{-4} , where a is the scale factor. From this perspective, ΔN_ν could either be positive or negative; the latter does not necessarily imply fewer than the standard-model number of neutrinos but could, for example, be a sign that the three standard-model neutrinos failed to be fully populated in the early Universe or, could reflect modifications to the $3 + 1$ dimensional Friedman equations arising from higher-dimensional extensions of the standard model of particle physics (Randall & Sundrum 1999; Binetruy et al. 2000; Cline et al. 2000).

3. N_ν AND η_B FROM BBN

The stage is being set for BBN when the Universe is about a tenth of a second old and the temperature is a few MeV. At this time the energy density of the universe is dominated by relativistic particles. When the temperature drops below ~ 2 MeV, the neutrinos begin to decouple from the photon- e^\pm plasma. However, they do continue to interact with the neutrons and protons through the charged-current weak interactions ($n + \nu_e \leftrightarrow p + e^-$, $p + \bar{\nu}_e \leftrightarrow n + e^+$, $n \leftrightarrow p + e^- + \bar{\nu}_e$), maintaining the neutron-to-proton ratio at its equilibrium value of $n/p = \exp(-\Delta m/kT)$, where Δm is the neutron-proton mass difference. When the temperature drops below ~ 0.8 MeV, and the Universe is ~ 1 second old, the reactions regulating the neutron-proton ratio become slower than the universal expansion rate ($\Gamma_{wk} < H$). As a result, the neutron-proton ratio deviates from (exceeds) its equilibrium value, so that $n/p > \exp(-\Delta m/kT)$, and the actual n/p ratio depends on the competition between the expansion rate (H) and the charged-current weak interaction rate (Γ_{wk}), as well as on the neutron decay rate, $1/\tau_n$, where τ_n is the neutron lifetime.

Although nuclear reactions such as $n + p \leftrightarrow D + \gamma$, proceed rapidly during these epochs, the large γ -ray background (the blue-shifted CMB) ensures that the deuterium (D) abundance is very small, inhibiting the formation of more complex nuclei. The more complex nuclei begin to form only when $T \lesssim 0.08$ MeV, after e^\pm annihilation, when the Universe is about 3 minutes old. At this time the number density of photons with sufficient energy to photodissociate deuterium is comparable to the baryon number density and various two-body nuclear reactions can begin to build more complex nuclei. Note that the neutron-to-proton ratio has decreased slightly since ‘‘freeze-out’’ (at $T \lesssim 0.8$ MeV) through the residual two body reactions as well as via beta decay. Once BBN begins neutrons and proton combine to form D, ${}^3\text{He}$, and ${}^4\text{He}$. The absence of a stable mass-5 nuclide presents a roadblock to the synthesis of heavier elements in the expanding, cooling Universe, ensuring that the abundances of heavier nuclides are severely depressed below those of the lighter nuclei. In standard BBN (SBBN) only D, ${}^3\text{He}$, ${}^4\text{He}$, and ${}^7\text{Li}$ are produced in astrophysically interesting abundances (for a recent review see Steigman (2007)). While the BBN-predicted abundances of D, ${}^3\text{He}$, and ${}^7\text{Li}$ are most sensitive to the baryon density, that of ${}^4\text{He}$ is very sensitive to the neutron abundance when BBN begins and, therefore, to the competition between the weak-interaction rate and the universal expansion rate. The primordial abundances of D, ${}^3\text{He}$, or ${}^7\text{Li}$ are baryometers, constraining η_B , while ${}^4\text{He}$ mass fraction (Y_P) is a chronometer, depending mainly on S or, N_ν . In the standard model of particle physics and cosmology with three species of neutrinos and their respective antineutrinos, the primordial element abundances depend on only one free parameter, the baryon density parameter, the post- e^\pm ratio (by number) of baryons to photons, $\eta_B = n_B/n_\gamma$. This parameter may be related to Ω_B , the present-Universe ratio of the baryon mass density to the critical mass-energy density (see Steigman (2006))

$$\eta_{10} = 10^{10} n_B/n_\gamma = 273.9 \Omega_B h^2. \quad (10)$$

The abundance of ${}^4\text{He}$ is very sensitive to the early expansion rate. Since a non-standard expansion rate ($S \neq 1$) would result in fewer or more neutrons at BBN and, since most neutrons are incorporated into ${}^4\text{He}$, the predicted ${}^4\text{He}$ abundance differs from that in SBBN ($S = 1$; $\Delta N_\nu = 0$). In contrast, the abundance of ${}^4\text{He}$ is not very sensitive to the baryon density since, to first order, all the neutrons available at BBN are rapidly converted to ${}^4\text{He}$. For $\eta_{10} \approx 6$, $N_\nu \approx 3$ and, for a primordial ${}^4\text{He}$ mass fraction in the range $0.23 \lesssim Y_P \lesssim 0.27$, to a very good approximation (Kneller & Steigman 2004; Steigman 2007),

$$Y_P = 0.2485 \pm 0.0006 + 0.0016[(\eta_{10} - 6) + 100(S - 1)]. \quad (11)$$

In eq. 11, the effect of incomplete neutrino decoupling on the ${}^4\text{He}$ mass fraction is accounted for according to Mangano et al. (2005) and S is related to ΔN_ν ($\Delta N_\nu \equiv N_\nu - 3.0$) by eq. 5. As a result, for a fixed ${}^4\text{He}$ abundance, a variation in η_{10} of $\sim \pm 0.2$ (corresponding to a $\sim 3\%$ uncertainty in the baryon density) is equivalent to an uncertainty in ΔN_ν of $\sim \pm 0.02$.

In contrast to ${}^4\text{He}$, since the primordial abundances of D, ${}^3\text{He}$ and ${}^7\text{Li}$ are set by the competition between two body production and destruction rates, they are more sensitive to the baryon density than to the expansion rate. For example, for $\eta_{10} \approx 6$ and for a primordial ratio of D to H by number, $y_D \equiv 10^5(\text{D}/\text{H})_P$, in the range, $2 \lesssim y_D \lesssim 4$, to a very good approximation (Kneller & Steigman 2004; Steigman 2007),

$$y_D = 2.64(1 \pm 0.03) \left[\frac{6}{\eta_{10} - 6(S - 1)} \right]^{1.6}. \quad (12)$$

The effect of incomplete neutrino decoupling on this prediction is at the $\sim 0.3\%$ level (Mangano et al. 2005), about ten times smaller than the overall error estimate above.

3.1. Observationally-Inferred Primordial Abundances

Given the monotonic post-BBN evolution of deuterium (as gas is cycled through stars, deuterium is destroyed) and the significant dependence of its predicted BBN abundance on the baryon density ($y_{DP} \propto \eta_{10}^{-1.6}$), deuterium is the baryometer of choice among the light nuclides produced during primordial nucleosynthesis. While observations of D/H in the solar system and the local interstellar medium provide a lower limit to the relic deuterium abundance, it is the D/H ratio (by number) measured from observations of high redshift, low metallicity QSO absorption line systems which provide an estimate of its primordial abundance. The weighted mean of the six, high redshift, low metallicity D/H ratios from Kirkman et al. (2003) and O’Meara et al. (2006) is (Steigman 2007)

$$y_{DP} = 2.68_{-0.25}^{+0.27}. \quad (13)$$

Since the post-BBN evolution of ${}^3\text{He}$ is more complex and model dependent than that of deuterium and, since ${}^3\text{He}$ is only observed in chemically-evolved H II regions in the Galaxy and, since the ${}^3\text{He}$ primordial abundance is only weakly dependent on the baryon density ($10^5({}^3\text{He}/\text{H}) \equiv y_{3P} \propto \eta_{10}^{-0.6}$), its role as a baryometer is limited.

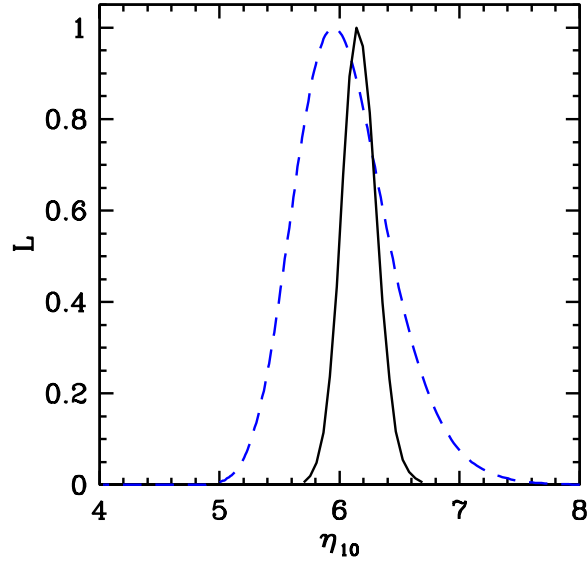


FIG. 1.— The probability distribution of the baryon density parameter, η_{10} . The dashed line shows the probability distribution inferred from SBBN ($N_\nu = 3$) and the adopted primordial abundance of deuterium (see §3). The solid line is the probability distribution of η_{10} inferred for $N_\nu = 3$ from the combination of the WMAP-5yr data, small scale CMB data, matter power spectrum data from 2dFGRS and SDSS LRG, SNIa, and the HST Key Project (see §4).

As for deuterium, the post-BBN evolution of ${}^4\text{He}$ is monotonic, with Y_P increasing along with increasing metallicity. At low metallicity, the ${}^4\text{He}$ abundance should approach its primordial value. As a result, it is the observations of helium and hydrogen recombination lines from low-metallicity, extragalactic H II regions which are most useful in determining Y_P . At present, corrections for systematic uncertainties (and their uncertainties) dominate estimates of the observationally-inferred ${}^4\text{He}$ primordial mass fraction and, especially, of its error. Following Steigman (2007), we adopt for our estimate here,

$$Y_P = 0.240 \pm 0.006. \quad (14)$$

While the central value of Y_P adopted here is low, the conservatively-estimated uncertainty is relatively large (some ten times larger than the uncertainty in the BBN-predicted abundance for a fixed baryon density). In this context, it should be noted that although very careful studies of the systematic errors in very limited samples of H II regions provide poor estimators of Y_P as a result of their uncertain and/or model-dependent extrapolation to zero metallicity, they are of value in providing a robust *upper bound* to Y_P . Using the results of Olive & Skillman (2004), Fukugida & Kawasaki (2006), and Peimbert et al. (2007), we follow Steigman (2007) in adopting,

$$Y_P < 0.251 \pm 0.002. \quad (15)$$

Although the BBN-predicted ${}^7\text{Li}$ relic abundance provides a potentially sensitive baryometer ($(\text{Li}/\text{H}) \propto \eta_{10}^2$, for $\eta_{10} \gtrsim 3$), its post-BBN evolution is complicated and model-dependent. For these reasons, it is the observations of lithium in the oldest, most metal-poor stars in galactic globular clusters and in the halo of the Galaxy which have the potential to provide the best estimate of the primordial abundance of ${}^7\text{Li}$. The complication associated with this approach is that these oldest galactic stars have had the most time to dilute or deplete their lithium surface abundances, leading to the possibility that the observed abundances require large, uncertain, and model-dependent corrections in order to infer the primordial abundance of ${}^7\text{Li}$. In the absence of corrections for depletion, dilution, or gravitational settling, the data of Ryan et al. (2000) and Asplund et al. (2006) suggest

$$[\text{Li}]_P \equiv 12 + \log(\text{Li}/\text{H}) = 2.1 \pm 0.1. \quad (16)$$

In contrast, in an attempt to correct for evolution of the surface lithium abundances, Korn et al. (2006) use their observations of a small, selected sample of stars in the globular cluster NGC6397, along with stellar evolution models which include the effect of gravitational settling to infer

$$[\text{Li}]_P = 2.54 \pm 0.1. \quad (17)$$

In the following analysis, the inferred primordial abundances of D and ${}^4\text{He}$ adopted here are used to estimate η_{10} and ΔN_ν . Given the inferred best values and uncertainties in these two parameters, the corresponding BBN-predicted abundance of ${}^7\text{Li}$ can be derived and compared to its observationally inferred abundance.

3.2. BBN Constraints On N_ν And η_B

Since the primordial abundance of deuterium is most sensitive to η_{10} , while that of ${}^4\text{He}$ is most sensitive to N_ν , isoabundance contours of D/H and Y_P in the $\{\eta_{10}, \Delta N_\nu\}$ plane are very nearly orthogonal; see Kneller & Steigman (2004). The analytic fits to BBN from Kneller & Steigman (2004), updated by Steigman (2007), are used in concert with the primordial abundances of D and ${}^4\text{He}$ adopted here to infer the best values, and to constrain the ranges of η_{10} and ΔN_ν . While these fits do have a limited range of applicability, they are, in fact, accurate within their quoted uncertainties for the range of parameter values and observed abundances considered here.

In SBBN, with three species of neutrinos ($\Delta N_\nu = 0$), the primordial abundances are only functions of the baryon density, η_B . For SBBN, the primordial deuterium abundance adopted in §3.1, $y_{\text{DP}} = 2.68^{+0.27}_{-0.25}$, implies,

$$\eta_{10}(\text{SBBN}) = 6.0 \pm 0.4 \quad (18)$$

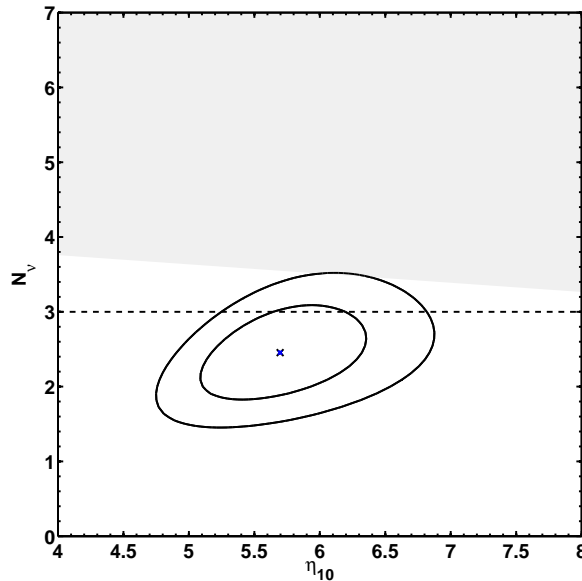


FIG. 2.— The 68% and 95% contours in the $N_\nu - \eta_{10}$ plane derived from a comparison of the observationally-inferred and the BBN-predicted primordial abundances of D and ${}^4\text{He}$. The shaded region is excluded by the 95% upper bound to the helium abundance in eq. 15 (see, eq. 20).

This result is in excellent agreement with the independent estimate of $\eta_{10} = 6.1^{+0.2}_{-0.1}$ from the CMB and LSS (discussed below in §4). The probability distributions of η_{10} inferred from SBBN and from the CMB and LSS are shown in Figure 1.

For non-standard BBN, with $\Delta N_\nu \neq 0$ ($S \neq 1$), there is a second free parameter, N_ν (or, S). In this case, in addition to y_{DP} , the ${}^4\text{He}$ abundance Y_{P} is used to constrain the $\{\eta_{10}, N_\nu\}$ pair. Adopting the D and ${}^4\text{He}$ abundances from §3.1 ($Y_{\text{P}} = 0.240 \pm 0.006$), along with the analytic fits in eq. (11) and eq. (12), leads to,

$$\eta_{10} = 5.7 \pm 0.4, \quad N_\nu = 2.4 \pm 0.4. \quad (19)$$

In Figure 2 are shown the 68% and 95% contours in the $N_\nu - \eta_{10}$ plane which follow from a comparison of the BBN predictions with the observationally-inferred primordial abundances of D and ${}^4\text{He}$. Notice that while the best fit value of N_ν is less than the standard-model value of $N_\nu = 3$, the standard-model value is consistent with the relic abundances at the $\sim 68\%$ level.

These results are sensitive to the choices of the relic abundances of D and ${}^4\text{He}$. We note that if deuterium is ignored and the robust upper bound to the ${}^4\text{He}$ mass fraction, $Y_{\text{P}} < 0.255$ at 95% confidence (eq. 15), is adopted, then eq. 11 provides an upper limit to S (N_ν) as a function of the baryon density,

$$S < 1.10 - 0.01\eta_{10}. \quad (20)$$

For η_{10} in the range $5 \leq \eta_{10} \leq 7$ (see §4), this corresponds to a robust upper bound to N_ν ranging from 3.6 to 3.4.

4. N_ν AND η_{B} FROM THE CMB AND LSS

The pattern of temperature fluctuations in the cosmic microwave background contain information about the baryon density and the radiation density and thus serve as complementary probes of η_{B} and N_ν some $\sim 10^5$ years after BBN.

The baryon density, parametrized by η_{B} or $\Omega_{\text{B}}h^2$ affects the relative amplitudes of the peaks in the CMB temperature power spectrum. The ratios of the amplitudes of the odd peaks to the even peaks provide a determination of η_{B} that is largely uncorrelated with N_ν .

The radiation density, parametrized by an effective number of neutrino species N_ν , affects the CMB power spectrum primarily through its effect on the epoch of matter-radiation equality. There are substantial differences in amplitudes between those scales that enter the horizon during the radiation dominated era and those that enter the horizon later, in the matter dominated era. Increasing the radiation content delays matter-radiation equality, bringing it closer to the epoch of recombination, suppressing the growth of perturbations. As a result, the redshift of the epoch of matter-radiation equality, z_{eq} , is a fundamental observable that can be extracted from the CMB Power Spectrum. z_{eq} is related to the matter and radiation densities by,

$$1 + z_{\text{eq}} = \rho_{\text{M}} / \rho_{\text{R}}. \quad (21)$$

Since ρ_{R} depends on N_ν , z_{eq} is a function of both N_ν and $\Omega_{\text{M}}h^2$, leading to a degeneracy between these two parameters. For a flat universe, preserving the fit to the CMB power spectrum when N_ν increases, requires that Ω_{M} and/or H_0 increase. As a result of this degeneracy, the CMB power spectrum alone imposes only a very weak constraint on N_ν (Crotty et al. 2003; Pierpaoli 2003; Barger et al. 2003; Hannestad 2003; Ichikawa et al. 2006). Inclusion of additional, independent constraints on these parameters are needed to break the degeneracy between N_ν and $\Omega_{\text{M}}h^2$.

Besides affecting the epoch of matter-radiation equality, relativistic neutrinos leave a distinctive signature on the CMB power spectrum due to their free streaming at speeds exceeding the sound speed of the photon-baryon fluid. This free streaming creates neutrino anisotropic stresses generating a phase shift of the CMB acoustic oscillations in both temperature and polarization. This phase shift is unique and, for adiabatic initial conditions, cannot be generated by non-relativistic matter. In principle, this effect can be used to break the degeneracy between N_ν and $\Omega_{\text{M}}h^2$, leading to tighter constraints on N_ν (Bashinsky & Seljak 2004).

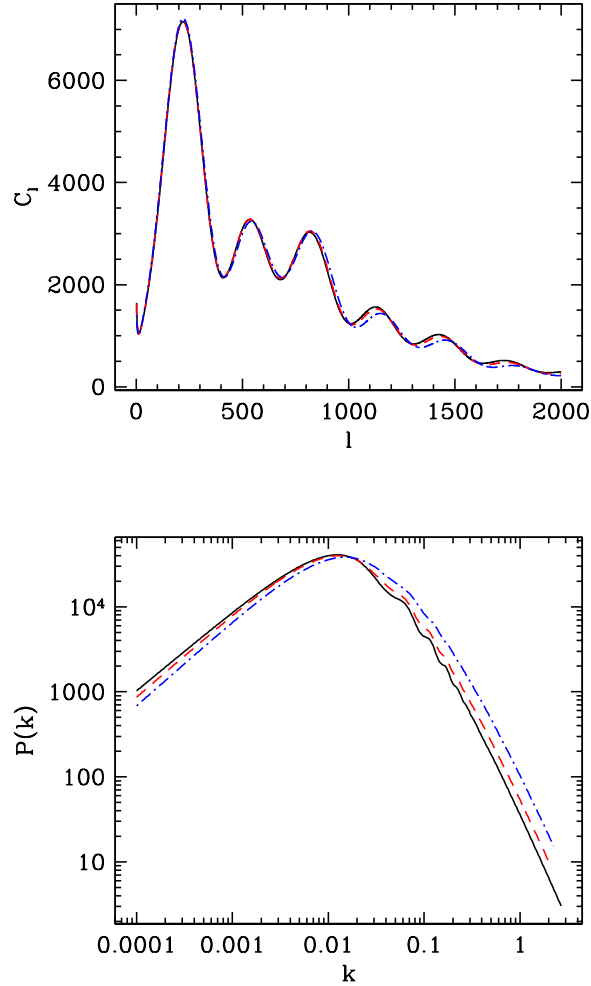


FIG. 3.— The top panel shows the CMB power spectrum for the best fit models with N_ν fixed at $N_\nu = 1$ (solid black), $N_\nu = 3$ (dashed red), and $N_\nu = 5$ (dot-dashed blue) illustrating its insensitivity to N_ν in the absence of an independent constraint on $\Omega_M h^2$. The bottom panel shows the matter power spectra for the same set of parameter values, illustrating its sensitivity to N_ν .

Alternatively, since the luminosity distances of type Ia supernovae (SNIa) provide a constraint on a combination of Ω_M and Ω_Λ complementary to that from the assumption of flatness, they are of value in restricting the allowed values of Ω_M . In concert with a bound on H_0 , this, too, helps to break the degeneracy between N_ν and $\Omega_M h^2$.

Another way to break the degeneracy between N_ν and $\Omega_M h^2$ is to use measurements of the matter power spectrum in combination with the CMB power spectrum. To preserve a fit to the CMB power spectrum, an increase in N_ν requires that $\Omega_M h^2$ increase in order that the redshift of matter-radiation equality remain unchanged. The turnover scale in the matter power spectrum is set by this connection between N_ν and $\Omega_M h^2$. Since the baryon density is constrained by the CMB power spectrum, independently of N_ν , increasing the radiation density ($N_\nu > 3$) requires a higher dark matter density in order to preserve z_{eq} (in a flat universe, $\Omega_M + \Omega_\Lambda = 1$). Between the epoch of matter-radiation equality and recombination the density contrast in the cold dark matter grows unimpeded, while the baryon density contrast cannot grow. Consequently, increasing N_ν and $\Omega_M h^2$, increases the amplitude of the matter power spectrum on scales smaller than the turnover scale corresponding to the size of the horizon at z_{eq} . Data from galaxy redshift surveys can be used to infer the matter power spectrum, thereby constraining $\Omega_M h^2$ and N_ν . This effect may be seen in Figure 3 which shows that for nearly indistinguishable CMB power spectra, different values of N_ν yield distinguishable matter power spectra. The upper panel of Figure 3 shows that by making suitable adjustments to the other cosmological parameters, specifically the matter density and the spectral index, CMB power spectra which are nearly degenerate up to the third peak of the power spectrum can be produced using very different values of N_ν . However, as the bottom panel of Figure 3 illustrates, these models produce matter power spectra with different shapes, demonstrating that the matter power spectrum can be used to help break the degeneracy between N_ν and $\Omega_M h^2$.

4.1. Analysis And Datasets

Before presenting our results, we describe the analysis and the datasets employed.

For our analysis we assume a flat, CDM cosmology with a cosmological constant, Λ , and three flavors of active neutrinos with negligible masses. Our cosmological model is parametrized by seven parameters:

$$p = \{\Omega_B h^2, \Omega_M h^2, h, \tau, n_S, A_S, N_\nu\}. \quad (22)$$

The contents of the universe are described by the baryon density, $\Omega_B h^2$ and the matter (baryonic plus cold dark matter) density,

$\Omega_M h^2$. Since a flat cosmology is assumed, the dark energy density and the matter density are related by $\Omega_\Lambda = 1 - \Omega_M$. The expansion rate of the universe is described by the reduced Hubble parameter, h ($H_0 = 100h \text{ kms}^{-1} \text{ Mpc}^{-1}$). Instantaneous reionization of the universe is assumed with optical depth to last scattering, τ . A_S is the amplitude of scalar perturbations and n_S is the scalar spectral index.

The Code for Anisotropies in the Microwave Background (CAMB) (Lewis et al. 2000) is used to compute the CMB power spectrum for a fixed set of cosmological parameters. For a given dataset, our degree of belief in a set of cosmological parameters $\{p\}$ is quantified by the posterior probability distribution,

$$P(p|data) \propto L(data|p) \Pi(p). \quad (23)$$

The likelihood $L(data|p)$ quantifies the agreement between the data and the set of parameter values $\{p\}$. $\Pi(p)$ represents the prior on cosmological parameter values before the data are considered.

Markov Chain Monte Carlo methods are used to explore the multi-dimensional likelihood surface. We use the publicly available COSMOMC code for our analysis (Lewis & Bridle 2002). Flat priors are adopted for all parameters, along with a prior on the age of the universe, t_0 , of $t_0 > 10 \text{ Gyr}$.

The *mode* of the marginalized posterior probability distribution is used as a point estimate and the *minimum credible interval* as an estimate of the uncertainty. The *minimum credible interval* selects the region of the parameter space around the mode, $\hat{\theta}$, that contains the appropriate fraction of the volume (e.g., 68%, 95%) of the posterior probability distribution, while minimizing $\hat{\theta} - \theta$. The *minimum credible interval* selects the region of the parameter space with the highest probability densities³.

Our primary dataset is the CMB data from the Wilkinson Microwave Anisotropy Probe (WMAP) accumulated from five years of observations (Hinshaw et al. 2008; Nolte et al. 2008). For the WMAP data, likelihoods are computed using the code provided on the LAMBDA webpage⁴. There are a number of ground and balloon based CMB experiments whose high angular resolution probe smaller scales than those probed by WMAP. These are more sensitive to the higher order acoustic oscillations beyond the third peak in the CMB power spectrum. In particular, the 2008 results from the Arcminute Cosmology Bolometer Array Receiver (ACBAR) (Reichardt et al. 2008) impose the strongest constraints at present on the CMB power spectrum at small angular scales. In our analysis, data from the following CMB experiments are used: BOOMERANG (Piacentini et al. 2006; Montroy et al. 2006), ACBAR (Reichardt et al. 2008), CBI (Readhead et al. 2004; Mason et al. 2003), VSA (Dickinson et al. 2004), MAXIMA (Hanany et al. 2000) and DASI (Halverson et al. 2001).

To help break the degeneracy between N_ν and $\Omega_M h^2$, we adopt a Gaussian prior on the Hubble parameter, $H_0 = 72 \pm 8 \text{ kms}^{-1} \text{ Mpc}^{-1}$ from the Hubble Space Telescope Key Project (Freedman et al. 2001).

Since the luminosity distances of type Ia supernovae (SNIa) provide a constraint on a combination of Ω_M and Ω_Λ , they are of value in restricting the allowed values of Ω_M , helping to break the degeneracy between N_ν and $\Omega_M h^2$. We use the luminosity distances for 115 type Ia supernovae measured by the Supernova Legacy Survey (SNLS) (Astier et al. 2006). For each supernova, the observed luminosity distance is compared to that predicted for a given set of cosmological parameters.

We use the matter power spectrum inferred from galaxy redshift surveys such as the Sloan Digital Sky Survey (SDSS) (Tegmark et al. 2004, 2006) and the 2dFGRS (Cole et al. 2005). In using the matter power spectrum to infer cosmological parameters, it has become clear that the constraint on Ω_M is sensitive to the choice of length scales on which the power spectrum is measured. The power spectrum on smaller scales prefers higher values of Ω_M , provided that those scales are correctly described by linear perturbation growth and scale independent galaxy bias (Cole et al. 2005; Percival et al. 2007). For example, using the SDSS LRG power spectrum (Tegmark et al. 2006) in combination with the 3 year WMAP dataset (Spergel et al. 2007), Dunkley et al. (2008) find a disagreement between the matter density inferred on scales with $k \leq 0.1h \text{ Mpc}^{-1}$ and $k \leq 0.2h \text{ Mpc}^{-1}$. Hamann et al. (2007) have shown that the constraint on N_ν obtained from the matter power spectrum is affected similarly, resulting from the correlation between Ω_M and N_ν . Therefore, here we only use matter power spectrum data on scales that are likely to be safely linear. We truncate the matter power spectrum at $k = 0.07h \text{ Mpc}^{-1}$, keeping data only on scales with $k \leq 0.07h \text{ Mpc}^{-1}$. We assume that galaxy bias is constant and scale independent for these scales.

4.2. N_ν And The Lyman- α Forest

Measurements of the flux power spectrum of the Lyman- α forest in QSO absorption spectra can be used to reconstruct the matter power spectrum on small scales (Croft et al. 1998; McDonald et al. 2000). Observations of the SDSS Ly- α flux power spectrum have been used to constrain the linear matter power spectrum at $z \sim 3$ (McDonald et al. 2005). When these constraints are combined with CMB power spectrum data, they favor considerably higher values of N_ν than those we find here (§5). For example, Seljak et al. (2006) found $N_\nu = 5.2$ and a 95% range $3.4 \leq N_\nu \leq 7.3$ and Hamann et al. (2007) found $N_\nu = 6.4$ and a 95% range $3.2 \leq N_\nu \leq 11$, the difference being accounted for by their different combinations of data sets. Each of these excludes the standard model value of $N_\nu = 3$ at more than 95% confidence.

As discussed earlier and shown in the lower panel of Figure 3, the principal effect of an increase in N_ν is to increase the amplitude of the matter power spectrum on scales smaller than those corresponding to the horizon at matter-radiation equality, z_{eq} . The Λ CDM fits to the Lyman- α forest data prefer higher amplitudes of density fluctuations on small scales compared to those expected from measurements of the WMAP power spectrum (Viel & Haehnelt 2006), favoring higher values of N_ν . This effect is seen in Figure 3 which shows that for nearly indistinguishable CMB power spectra, different values of N_ν yield distinguishable matter power spectra. To preserve z_{eq} and the fit to the CMB, the model with $N_\nu = 1$ has a lower value of $\Omega_M h^2$ and, therefore,

³ The commonly used GETDIST analysis package uses the mean of the marginalized posterior probability distribution as a point estimate and gives uncertainty estimates based on the *central credible interval* (Hamann et al. 2007). These estimates are identical for Gaussian probability distributions but differ significantly for non-Gaussian distributions, particularly for asymmetric probability distributions.

⁴ <http://lambda.gsfc.nasa.gov>

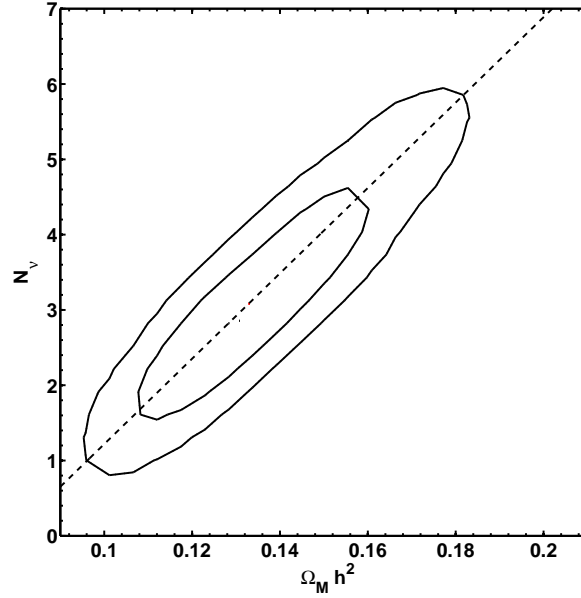


FIG. 4.— The 68% and 95% contours in the N_ν - $\Omega_M h^2$ plane inferred from the combination of the WMAP-5yr data, small scale CMB data, luminosity distances of SNIa and the HST Key Project prior on H_0 . The dashed line shows the locus of points corresponding to the same value of $z_{eq}(= 3144)$, illustrating the degeneracy between these two parameters. As the contours reveal, this degeneracy may be broken if complementary data is used to constrain $\Omega_M h^2$.

the matter power spectrum for that model has a lower amplitude on scales smaller than the scale corresponding to the horizon at the epoch of matter-radiation equality. Conversely, the model with $N_\nu = 5$ has a higher value of $\Omega_M h^2$ and the matter power spectrum for that model has a higher amplitude on scales smaller than the scale corresponding to the horizon at z_{eq} .

Before reaching any conclusions about N_ν based on the Lyman- α forest data, it is worth noting that assumptions about the thermal state of the IGM play an important role in reconstructing the matter power spectrum from the Lyman- α forest flux power spectrum. Bolton et al. (2007) compare measurements of the Lyman- α forest flux probability distribution by Kim et al. (2007) to hydrodynamic simulations of the Lyman- α forest, finding evidence for an *inverted* temperature-density relation for the low density intergalactic medium. Bolton et al. (2007) suggest that He II reionization could be a possible physical mechanism for achieving an inverted temperature-density relation. Such an inversion would result in a smaller amplitude of the matter power spectrum for a given observed flux power spectrum, thereby alleviating the tension with the other data sets which tended to drive N_ν to high values. However, in their power spectrum fits McDonald et al. (2005) marginalize over equation of state parameters, so this explanation of the tension may not be entirely satisfactory. Future studies of the Lyman- α forest may weaken or strengthen the evidence for a discrepancy. For these reasons, we do not use data from the Lyman- α forest in our analysis.

4.3. CMB And LSS Constraints On N_ν And η_B

According to Dunkley et al. (2008) the WMAP 5 year data only impose a lower limit on N_ν of $N_\nu > 2.3$ but, according to Komatsu et al. (2008), do not lead to an upper limit due to the degeneracy between N_ν and $\Omega_M h^2$. Inclusion of data from small scale CMB experiments do not break this degeneracy. Figure 4 illustrates this degeneracy, as well as how it may be broken by non-CMB constraints on $\Omega_M h^2$. The dashed line in Fig. 4 is the locus of points with constant $z_{eq} = 3144$. Figure 4 shows the joint probability distributions of N_ν and $\Omega_M h^2$ inferred from the WMAP 5yr data and small scale CMB experiments, supplemented by independent data from measurements of SNIa luminosity distances and the HST Key Project prior on H_0 are used to bound $\Omega_M h^2$. The range of N_ν is now limited.

Our constraints on N_ν and η_{10} from various CMB and LSS datasets and combinations of them are summarized in Table 1 and in Figures 5 – 7.

Using the WMAP 5 year data in combination with data from other CMB experiments (ACBAR, BOOMERANG, CBI, DAS1, MAXIMA and VSA), along with the HST Key Project prior on H_0 and luminosity distance measurements of type Ia supernovae, we find central values $N_\nu = 2.9$ and $\eta_{10} = 6.2$, along with 68% (95%) ranges of $2.0 < N_\nu < 4.1$ ($1.3 < N_\nu < 5.4$) and $6.0 < \eta_{10} < 6.3$ ($5.9 < \eta_{10} < 6.4$). Figure 5 shows the joint probability distribution of N_ν and η_{10} for this combination of CMB datasets.

Adding the 2dFGRS power spectrum (Cole et al. 2005) to the CMB power spectrum from the WMAP 5 year dataset, along with ground based CMB experiments (see above), the HST prior on H_0 and, luminosity distance measurements from SNIa, we find central values $N_\nu = 3.0$ and $\eta_{10} = 6.1$, along with 68% (95%) ranges $2.1 < N_\nu < 4.2$ ($1.3 < N_\nu < 5.2$) and $6.0 < \eta_{10} < 6.3$ ($5.9 < \eta_{10} < 6.4$) respectively; see Table 1. Replacing the 2dFGRS power spectrum with the SDSS LRG power spectrum (Tegmark et al. 2006), we obtain very similar results: $N_\nu = 2.8$, $2.1 < N_\nu < 3.9$ ($1.5 < N_\nu < 5.2$) and, $\eta_{10} = 6.2$, $6.1 < \eta_{10} < 6.3$ ($5.9 < \eta_{10} < 6.5$). In contrast, the SDSS DR2 (Tegmark et al. 2004) power spectrum favours considerably higher values of N_ν compared to those inferred from the 2dFGRS and the SDSS (LRG) power spectra.

Our best constraints on N_ν and η_{10} from the CMB and LSS data are derived by combining the following datasets - WMAP 5-year data, ground and balloon based CMB experiments (BOOMERANG, ACBAR, CBI, VSA, MAXIMA and DAS1), the HST prior on H_0 , the SNIa luminosity distance measurements and, the matter power spectrum on large scales inferred from the 2dFGRS and SDSS (LRG) data. Constraints on the matter power spectrum from the Lyman- α forest are not included for the

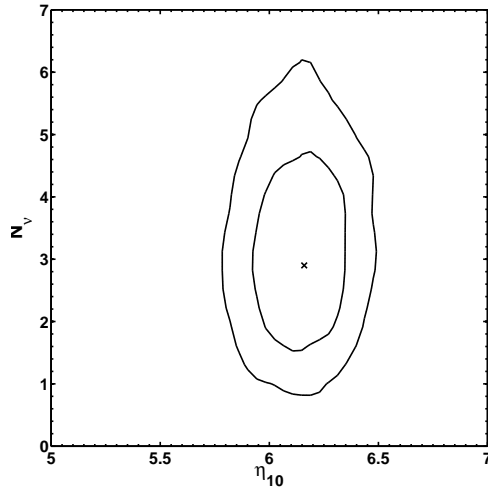


FIG. 5.— The 68% and 95% contours in the $N_\nu - \eta_{10}$ plane inferred from the combination of the WMAP-5yr data, small scale CMB data, SNIa luminosity distances, and the HST Key Project prior on H_0 (see the text and Table 1).

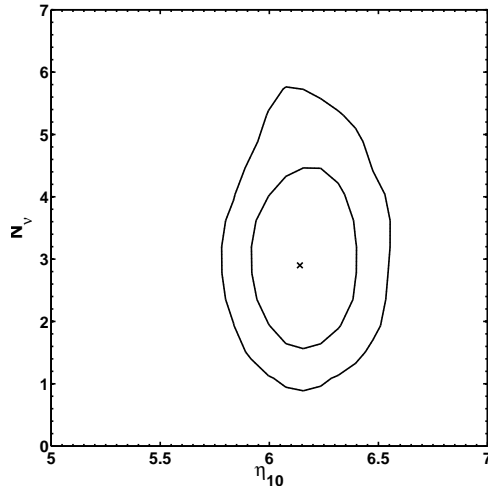


FIG. 6.— The 68% and 95% contours in the $N_\nu - \eta_{10}$ plane derived using the WMAP 5-year data, small scale CMB data, SNIa and the HST Key Project prior on H_0 along with matter power spectrum data from 2dFGRS and SDSS LRG (see the text and Table 1).

reasons discussed above in §4.2. Using these datasets, we obtain (see Table 1):

$$\eta_{10} = 6.1^{+0.2+0.3}_{-0.1-0.2}. \quad (24)$$

$$N_\nu = 2.9^{+1.0+2.0}_{-0.8-1.4}. \quad (25)$$

At present the combined CMB and LSS data provide the best baryometer, determining the baryon density to better than 3%, but only a relatively weak chronometer, still allowing a large range in S ($0.87 \leq S \leq 1.14$ at 95% confidence). Within their uncertainties, the CMB/LSS data, which probe the Universe at $\gtrsim 400,000$ years, are consistent with BBN, which provides a window on the Universe at $\lesssim 20$ minutes.

5. COMPARING THE BBN AND CMB/LSS CONSTRAINTS

Using the ranges of η_{10} and N_ν allowed by the CMB and LSS data, the BBN-predicted primordial abundances of ^4He , D and ^7Li may be inferred. Figure 8 compares these constraints to the observationally-inferred primordial abundances adopted in §3.1. The CMB/LSS-inferred BBN abundances of D and ^4He are in excellent agreement, within the errors, with the observationally-inferred relic abundances. For the central values of $\eta_{10} = 6.14$ and $N_\nu = 2.9$, the BBN-predicted deuterium abundance of $y_{\text{DP}} = 2.54$ is, within the errors, in agreement with its observationally-inferred primordial value of $y_{\text{DP}} = 2.68$. For ^4He , the BBN-predicted mass fraction is $Y_{\text{p}} = 0.247$, slightly high compared to the central value of the primordial abundance adopted in §3.1, $Y_{\text{p}} = 0.240$, but within 1.2σ of it and, completely consistent with the evolution-model independent upper bound presented in eq. 15, $Y_{\text{p}} < 0.251 \pm 0.002$.

For ^7Li the BBN-predicted best fit from the CMB/LSS data is $[\text{Li}]_{\text{p}} = 2.66$, considerably higher than the value ($[\text{Li}]_{\text{p}} = 2.1 \pm 0.1$) determined from observations of metal-poor halo stars (Ryan et al. (2000), Asplund et al. (2006)) without any correction for depletion, destruction, or gravitational settling. If, however, the correction proposed by Korn et al. (2006) is applied, the predicted and observed ^7Li abundances may, perhaps, be reconciled, as may be seen from the lower panel of Fig. 8. It remains an open question whether this lithium problem is best resolved by a better understanding of stellar physics or, if it is providing a hint of new physics beyond the standard model.

TABLE 1
 N_ν AND η_{10} FROM DIFFERENT DATASETS

Dataset	N_ν	η_{10}
BBN (Y_p & y_{DP})	$2.4^{+0.4+0.9}_{-0.4-0.8}$	$5.7^{+0.4+0.8}_{-0.4-0.9}$
WMAP(1yr)+HST	$2.8^{+4.5+5.5}_{-1.8-1.9}$	$6.1^{+0.5+1.8}_{-0.3-0.7}$
WMAP(3yr)+HST+SN	$2.9^{+2.1+4.0}_{-1.2-2.1}$	$6.06^{+0.23+0.42}_{-0.20-0.39}$
WMAP(3yr)+CMB(07)+HST+SN	$2.5^{+1.7+3.8}_{-1.2-1.7}$	$6.13^{+0.21+0.39}_{-0.18-0.36}$
2dFGRS+WMAP(3yr)+CMB(07)+HST+SN	$2.9^{+1.4+2.3}_{-1.2-2.3}$	$6.11^{+0.20+0.38}_{-0.15-0.32}$
SDSS(DR2)+WMAP(3yr)+CMB(07)+HST+SN	$3.7^{+1.6+3.3}_{-1.4-2.4}$	$6.15^{+0.15+0.35}_{-0.20-0.39}$
SDSS(LRG)+WMAP(3yr)+CMB(07)+HST+SN	$2.0^{+1.2+2.6}_{-1.2-1.8}$	$6.12^{+0.19+0.36}_{-0.16-0.34}$
WMAP(5yr)+HST+SN	$3.9^{+2.0+4.5}_{-1.2-2.4}$	$6.11^{+0.16+0.33}_{-0.16-0.33}$
WMAP(5yr)+CMB+HST+SN	$2.9^{+1.2+2.5}_{-0.9-1.6}$	$6.16^{+0.14+0.25}_{-0.16-0.30}$
2dFGRS+WMAP(5yr)+CMB+HST+SN	$3.0^{+1.2+2.2}_{-0.9-1.7}$	$6.14^{+0.16+0.27}_{-0.14-0.25}$
SDSS(LRG)+WMAP(5yr)+CMB+HST+SN	$2.8^{+1.1+2.4}_{-0.7-1.3}$	$6.16^{+0.14+0.27}_{-0.14-0.27}$
SDSS(LRG)+2dFGRS+WMAP(5yr)+CMB+HST+SN	$2.9^{+1.0+2.0}_{-0.8-1.4}$	$6.14^{+0.16+0.30}_{-0.11-0.25}$
BBN+SDSS(LRG)+2dFGRS+WMAP(5yr)+CMB+HST+SN	$2.5^{+0.4+0.7}_{-0.4-0.7}$	$6.11^{+0.12+0.26}_{-0.13-0.27}$

NOTE. — Best fits and 68% and 95% confidence intervals for N_ν and η_{10} from our principal datasets. WMAP refers to the CMB power spectrum data from the WMAP experiment and CMB to the data from ACBAR+BOOM+CBI+VSA+MAXIMA+DASI. CMB(07) uses the 2007 ACBAR dataset (Kuo et al. 2007) while CMB uses the 2008 ACBAR dataset (Reichardt et al. 2008). HST refers to the prior on H_0 from the HST Key Project. SN stands for the SNIa luminosity distance measurements. SDSS (LRG) and 2dF refer to the respective LSS matter power spectra, truncated at $k = 0.07h \text{ Mpc}^{-1}$.

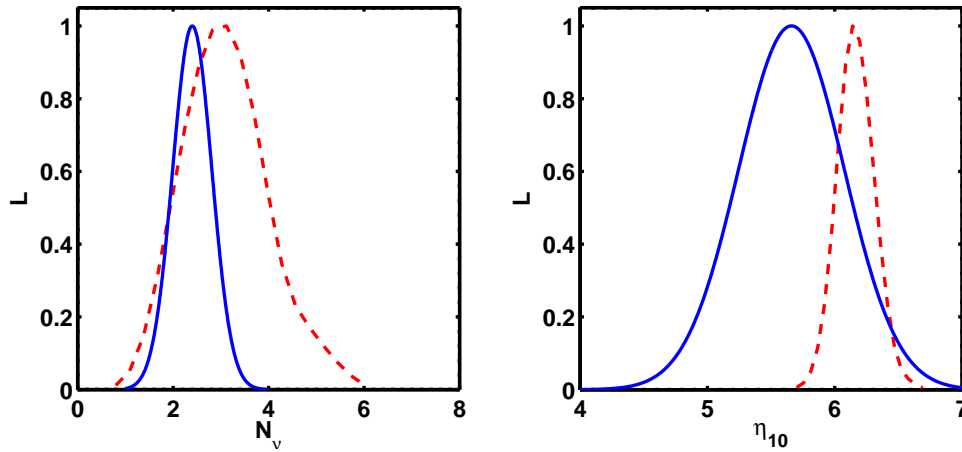


FIG. 7.—

On the left (red, dashed), the probability distribution of N_ν inferred from the combination of the WMAP 5-year data, small scale CMB data, SNIa and the HST Key Project prior on H_0 and matter power spectrum data from 2dFGRS and SDSS LRG. The solid blue curve is the BBN (D plus ^4He) distribution. On the right (same line types and colors), are the probability distributions of η_{10} using the same data sets.

6. CONCLUSIONS

While our CMB+LSS constraints on η_B and N_ν are consistent with most previous analyses (Crotty et al. 2003; Pierpaoli 2003; Hannestad 2003; Barger et al. 2003; Seljak et al. 2006; Ichikawa et al. 2006; Spergel et al. 2007; Mangano et al. 2007; Hamann et al. 2007; Dunkley et al. 2008; Komatsu et al. 2008), they are tighter because we have used more and/or more recent data. However, as discussed above in §4.2, analyses that included the Lyman- α forest data generally find higher values of N_ν .

Until the advent of WMAP and the other ground- and balloon-based CMB experiments, BBN provided the best baryometer (mainly from deuterium) and chronometer (mainly from helium-4). As may be seen from Table 1, while the WMAP first year data provided a competitive baryometer, it offered a relatively poor chronometer. This improves with the WMAP 3 and 5 year data, especially when they are combined with the other CMB and LSS data. These now lead to a determination of the baryon density at the $\sim 2-3\%$ level, a factor of $\gtrsim 2$ better than that from BBN. However, although the CMB/LSS constraint on N_ν has improved significantly and, it is consistent with that from BBN, it remains weaker than the BBN constraint by a factor of ~ 2 . For some time now BBN has clearly established at high confidence that $N_\nu > 1$ when the Universe was ~ 20 minutes old. For example, using a slightly different estimate of the primordial helium mass fraction, Barger et al. (2003) found $N_\nu > 1.7$ at 95% confidence (see also Steigman (2006a)). The more recent WMAP 5 year data, combined with the recent ACBAR and other CMB

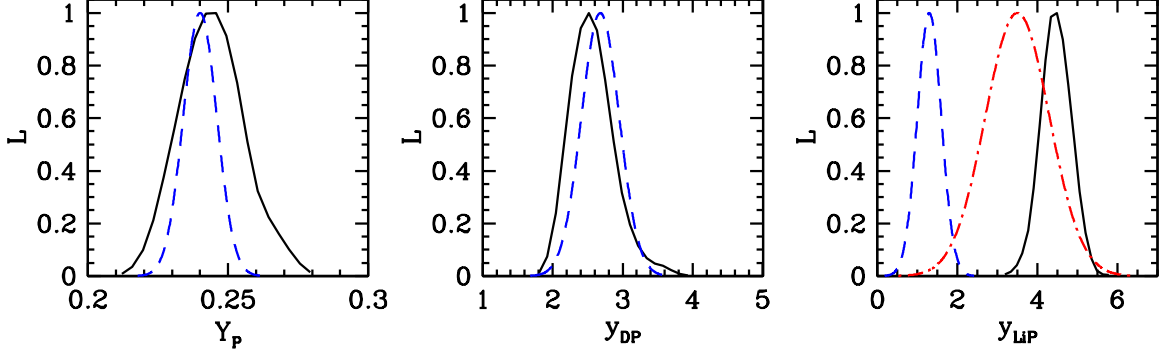


FIG. 8.—

The solid black curves show the probability distributions for the primordial abundances of D, ${}^4\text{He}$ and ${}^7\text{Li}$ derived from the values of η_{10} and N_ν inferred from the CMB, LSS, SNIa and the HST prior and matter power spectrum data from 2dFGRS and SDSS LRG. The blue dashed curves show the probability distributions for the observationally-inferred primordial abundances of D, ${}^4\text{He}$ and ${}^7\text{Li}$; see §3.1. The red, dot-dashed curve in the far right panel is the ${}^7\text{Li}$ abundance from Korn et al. (2006).

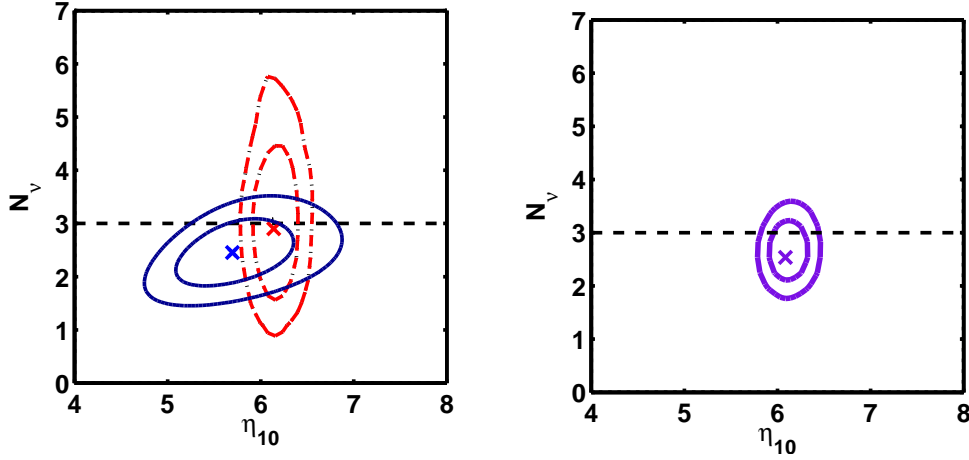


FIG. 9.—

(Left) In blue (solid), the 68% and 95% contours in the $N_\nu - \eta_{10}$ plane derived from a comparison of the observationally-inferred and BBN-predicted primordial abundances of D and ${}^4\text{He}$ (see Figure 2). In red (dashed), the 68% and 95% contours derived from the combined WMAP 5-year data, small scale CMB data, SNIa, and the HST Key Project prior on H_0 along with matter power spectrum data from 2dFGRS and SDSS LRG (see the text and Table 1). (Right) The 68% and 95% joint BBN-CMB-LSS contours in the $N_\nu - \eta_{10}$ plane.

and LSS datasets, the CMB/LSS now confirm that $N_\nu > 1$ (or, $N_\nu > 2$ (Dunkley et al. 2008)) when the Universe was $\gtrsim 400$ kyr old.

As may be seen from Table 1 and from Figures 7, 8, and from the left-hand panel of Figure 9, BBN and the CMB, which probe physics at widely separated epochs in the evolution of the Universe, are in excellent agreement. This permits constraints on any *differences* in physics between BBN and recombination and/or the present epoch. For example, since baryons are conserved, η_B relates the number of thermalized black body photons in a comoving volume at different epochs (see figure 7), constraining any post-BBN entropy production. Our results from the CMB/LSS and from BBN imply,

$$\frac{N_\gamma^{\text{CMB}}}{N_\gamma^{\text{BBN}}} = 0.92 \pm 0.07. \quad (26)$$

This ratio is consistent with 1 at $\sim 1\sigma$ and places an interesting upper bound on any post-BBN entropy production.

Alternatively, late decaying particles could produce relativistic particles (radiation), but not necessarily thermalized black body photons (see, for example, Ichikawa et al. (2007)). Deviations from the standard model radiation density can be parametrized by the ratio of the radiation density, ρ'_R to the standard model radiation density, ρ_R . In the post- e^\pm annihilation universe (see eq. 9),

$$R = S^2 = \frac{\rho'_R}{\rho_R} = 1 + 0.134 \Delta N_\nu. \quad (27)$$

Comparing this ratio, at BBN and at recombination (see figure 7), any post-BBN production of relativistic particles can be constrained.

$$\frac{R_{\text{CMB}}}{R_{\text{BBN}}} = 1.07^{+0.16}_{-0.13} \quad (28)$$

This ratio, too, is consistent with 1 within 1σ , placing an upper bound on post-BBN production of relativistic particles.

Although the non-standard expansion rate has been parametrized in terms of an equivalent number of additional species of neutrinos, we have emphasized that a non-standard expansion rate need not be related to extra (or fewer) neutrinos. For example, deviations from the standard expansion rate could occur if the value of the early-Universe gravitational constant, G_N were different from its present, locally-measured value (Yang et al. 1979; Boesgaard & Steigman 1985; Accetta et al. 1990; Cyburt et al. 2005). For the standard radiation density with three species of light, active neutrinos, the constraint on the expansion rate can be used to constrain variations in the gravitational constant, G_N . From BBN,

$$S^2 = \frac{G_N^{\text{BBN}}}{G_N} = 0.91 \pm 0.07 \quad (29)$$

and at the epoch of the recombination,

$$S^2 = \frac{G_N^{\text{CMB}}}{G_N} = 0.99^{+0.13}_{-0.11}, \quad (30)$$

consistent with no variation in G at the $\sim 1\sigma$ level.

The agreement between η_B and N_ν evaluated from BBN (~ 20 minutes) and from the CMB/LSS ($\gtrsim 400$ kyr) is shown in the left hand panel of Figure 9. As Figure 9 illustrates, BBN and the CMB/LSS, which probe the Universe at widely separated epochs in its evolution, are completely consistent. As already noted, at present the CMB is a better baryometer while BBN remains a better chronometer. Since these independent constraints from the CMB/LSS and BBN are in very good agreement, we may combine them to obtain the joint fit in Table 1 and shown in the right hand panel of Figure 9. We note that while the best-fit value of N_ν is less than 3, this is not statistically significant since the results are consistent with the standard model of three species of active neutrinos at the $\sim 1\sigma$ level.

Of course, our BBN results are sensitive to the relic abundances we have adopted. For comparison, we have repeated our analysis for an alternate set of primordial abundances. For deuterium, we adopted the O’Meara et al. (2006) results based on the weighted mean of the $\log(y_D)$ values, $y_D = 2.84^{+0.27}_{-0.25}$ and, for ${}^4\text{He}$ we chose, somewhat arbitrarily, $Y_p = 0.247 \pm 0.004$. For this alternate abundance set the BBN-predicted value of η_B is virtually unchanged from our previous result, $\eta_{10} = 5.7 \pm 0.3$, while $N_\nu = 2.9 \pm 0.3$ is much closer to the standard model expectation. As a result, while the constraint on entropy production (eq. 26) is unchanged, $R_{\text{CMB}}/R_{\text{BBN}} = 1.00^{+0.16}_{-0.13}$ and $G_N^{\text{BBN}}/G_N = 0.99^{+0.13}_{-0.11}$. When the alternate BBN constraints are combined with those from the CMB and LSS, we find $\eta_{10} = 6.09^{+0.12}_{-0.13}$ and $N_\nu = 2.9 \pm 0.3$.

Very recent observations of deuterium in the high redshift, low metallicity Damped Lyman- α absorber by Pettini et al. (2008) lead to a deuterium abundance very close to the mean of the previous six abundances used in this paper. As a result, the change in y_D is very small ($y_D = 2.70$ rather than $y_D = 2.68$ adopted in this paper). Consequently, the change in the parameters inferred from it (N_ν and η_{10}) is also very small.

Future CMB experiments will improve the constraint on N_ν by measuring the neutrino anisotropic stress more accurately. According to Bashinsky & Seljak (2004), PLANCK should determine N_ν to an accuracy of $\sigma(N_\nu) \sim 0.24$ and CMBPOL, a satellite based polarization experiment, might improve it further to $\sigma(N_\nu) \sim 0.09$, independent of the BBN constraints. In this context, we note that such tight constraints on N_ν will be sensitive to the value of the ${}^4\text{He}$ abundance adopted in the CMB analysis. To achieve these projected accuracies, it will no longer be sufficient to fix Y_p in advance. Rather, Y_p should be solved for in concert with the other cosmological parameters. To this end, we point out that for $\eta_{10} \approx 6$, $N_\nu \approx 3$ (suggested by our results), a very good, simple approximation to Y_p is provided by eq. 11 (Kneller & Steigman 2004; Steigman 2007).

ACKNOWLEDGMENTS

This research is supported at The Ohio State University by a grant (DE-FG02-91ER40690) from the US Department of Energy. We thank D. Weinberg for a careful reading of the manuscript and for suggestions which led to an improved manuscript. We also thank R. Cyburt, S. Dong, J. Dunkley, J. Hamann, S. Hannestad, A. Lewis, P. McDonald, M. Pettini, G. Raffelt, and Y. Wong for useful discussions. We thank the Ohio Supercomputer Center for the use of a Cluster Ohio Beowulf cluster in this research.

REFERENCES

- Accetta, F.S., Krauss, L.M. & Romanelli, P. 1990, Phys. Lett. B 248, 146.
 Asplund, M. et al. 2006, ApJ, 644,229.
 Astier, P. et al. 2006, Astron. & Astrophys. 447, 31.
 Barger V, Kneller J.P., Lee H-S, Marfatia D, and Steigman G 2003, Phys. Lett. B, 569, 123.
 Bashinsky, S., Seljak, U. 2004, Phys. Rev. D69, 083002.
 Bania, T.M. et al. 2002, Nature 415, 54.
 Binetruy, P., Deffayet, C., Ellwanger, U. & Langlois, D. 2000, Phys. Lett. B, 477, 285.
 Boesgaard, A.M., & Steigman, G. 1985, Ann. Rev. Astron. Astrophys., 23, 319.
 Bolton, J.S. et al. 2007, arXiv:0711.2064v1
 Bowen, R. et al. 2002, MNRAS, 334, 760.
 Cline, J. M., Grojean, C. & Servant, G. 2000, PRL, 83, 4245.
 Cole, S. et al.(2005), MNRAS, 362, 505.
 Croft, R.A.C. et al.(1998), ApJ, 495, 44.
 Crotty, P., Lesgourges, J. & Pastor, S.(2003), Phys. Rev. D67, 123005.
 Cyburt, R.H.(2004), Phys. Rev. D, 70, 023505.
 Cyburt, R.H. et al.(2005), Astropart. Phys. 23, 313
 Dicus, D. A., et al. 1982, Phys. Rev. D26, 2694.
 Dodelson, S. & Turner, M. S. 1992, Phys. Rev. D46, 3372.
 Dolgov, A. D., 2002, Phys. Rep., 370, 333.
 Dickinson, C., et al. 2004, MNRAS, 353, 732.
 Dunkley, J., et al. 2008, arXiv:0803.0586
 Freedman, W.L. et al. 2001, ApJ, 553, 47.
 Fukugida, M. & Kawasaki, M. 2006, ApJ, 646, 691.
 Halverson, N.W., et al. 2001, ApJ, 568, 38.
 Hamann, J et al. 2007, JCAP, 0708, 021
 Hanany, S et al. 2000, ApJ, 545, L5.
 Hannestad, S. & Madsen, J. 1995, Phys. Rev. D52, 1764.
 Hannestad, S. 2003, JCAP, 0305, 004
 Hinshaw, G., et al. 2008, arXiv:0803.0732.
 Ichikawa, K., Kawasaki, M. & Takahashi, M, 2006, JCAP, 0705, 007.
 Ichikawa, K. et al. 2007 JCAP 0705, 008.
 Izotov, I.T. & Thuan, T.X. 2004, ApJ, 602, 200.
 Kim, T.S. et al. 2007 arXiv:0711.1862
 Kirkman, D et al. 2003 ApJS, 149, 1.
 Kneller J P and Steigman G 2004, New J. Phys., 6, 117.

- Komatsu, E., et al. 2008, arXiv:0803.0547
Korn, A.J. et al. 2006, Nature, 442, 657.
Kuo, et al. 2007, ApJ, 600,32.
Lewis, A. et al. 1999, ApJ, 538, 473.
Lewis, A. & Bridle, S. 2002, Phys. Rev. D, 66, 103511.
Lopez, R. E., Dodelson, S., Heckler, A. & Turner, M. S. 1999, PRL, 82, 3952.
Mangano, G. et al. 2005, Nucl.Phys. B729, 221.
Mangano, G. et al. 2007, JCAP, 0703, 006.
Mason, B. S., et al. 2003, ApJ, 591, 540.
McDonald, P. et al. 2000, ApJ, 543, 1.
McDonald, P. et al. 2006, ApJ, 635, 761.
Montroy, T.E., et al. 2006, ApJ, 647, 813.
Nolta, M.R., et al. 2008, arXiv:0803.0593.
Olive, K. A. & Skillman, E. D. 2004, ApJ, 617, 29.
O'Meara, J. M. et al. 2006, ApJL, 649, L61.
Peimbert, M., Luridiana, V., Peimbert, A. 2007, ApJ, 666, 636.
Percival, W.J. et al. 2007, ApJ, 645, 663.
Pettini, M. et al. 2008, arXiv:0805.0594
Piacentini, F. et al. 2006, ApJ, 647, 833.
Pierpaoli, E. 2003, MNRAS, 342, L63.
Randall, L. & Sundrum, R. 1999a, PRL, 83, 3370; *ibid* 1999b, PRL, 83, 4690.
Readhead, A.C.S., et al. 2004, ApJ, 609, 498
Reichardt, C.L. et al. 2008, arXiv:0801.1491
Reiss, A.G. et al. 2004, ApJ, 607, 655.
Ryan, S.G et al. 2000, ApJ, 530, L57.
Seljak, U., Slosar, A., McDonald, P. 2006, JCAP, 0610, 014.
Spergel D. N. et al. 2003, ApJ Suppl., 148, 175.
Spergel, D. N. et al. 2007, ApJS, 170, 377.
Steigman, G. 2006, JCAP, 10, 016.
Steigman, G. 2006, IJMPE, 15, 1.
Steigman, G. 2007, Ann. Rev. Nucl. Part. Sci., 57, 463.
Tegmark, M. et al. 2004, ApJ, 606, 702.
Tegmark, M. et al. 2006, Phys. Rev. D74, 123507.
Viel, M. & Haehnelt, M.G. 2006, MNRAS, 365, 231.
Yang, J.M., Schramm, D.N., Steigman, G. & Rood, R.T. 1979, ApJ, 227, 697.